ARTICLE

doi:10.1038/nature13293

Crystal structure of a human $GABA_A$ receptor

Paul S. Miller[1] & A. Radu Aricescu[1]

Type-A γ-aminobutyric acid receptors ($GABA_A$Rs) are the principal mediators of rapid inhibitory synaptic transmission in the human brain. A decline in $GABA_A$R signalling triggers hyperactive neurological disorders such as insomnia, anxiety and epilepsy. Here we present the first three-dimensional structure of a $GABA_A$R, the human β3 homopentamer, at 3 Å resolution. This structure reveals architectural elements unique to eukaryotic Cys-loop receptors, explains the mechanistic consequences of multiple human disease mutations and shows an unexpected structural role for a conserved N-linked glycan. The receptor was crystallized bound to a previously unknown agonist, benzamidine, opening a new avenue for the rational design of $GABA_A$R modulators. The channel region forms a closed gate at the base of the pore, representative of a desensitized state. These results offer new insights into the signalling mechanisms of pentameric ligand-gated ion channels and enhance current understanding of GABAergic neurotransmission.

In response to binding the neurotransmitter GABA, released at inhibitory synapses, $GABA_A$R chloride channels open and depress neuronal excitability in the adult central nervous system[1]. $GABA_A$Rs belong to a superfamily of pentameric ligand-gated ion channels (pLGICs) known as the Cys-loop receptors, which includes the cation-selective nicotinic acetylcholine receptors (nAChRs) and serotonin type 3 receptors ($5HT_3$Rs), as well as anion-selective glycine receptors (GlyRs)[2]. These molecules assemble as pentamers from a variety of subunits. In human $GABA_A$Rs these subunits are encoded by 19 different genes: α1–6, β1–3, γ1–3, δ, ε, θ, π and ρ1–3 (ref. 3). Most physiological heteromeric formats are thought to include two α, two β and one other, most frequently a γ subunit[4]. β3 subunits can also efficiently assemble into functional homomeric channels, and although they have yet to be identified as discrete populations in the brain, they serve as meaningful models for the heteromeric receptors[5]. Each subunit contributes an extracellular domain of 200–250 amino acids, an α-helical M1–M4 transmembrane bundle and an M3–M4 intracellular loop of 85–255 residues[6]. Neurotransmitter molecules bind at extracellular pockets between subunits to induce a conformational switch that crosses to the transmembrane region to open the ion channel[7]. $GABA_A$Rs are the targets of a wide range of drugs including benzodiazepines[8], used in the treatment of epilepsy, insomnia, anxiety and panic disorder, and the intravenous general anaesthetics propofol and etomidate[5,9]. $GABA_A$Rs also mediate alcohol inebriation[10] and are targets for endogenous modulators such as neurosteroids[11].

In the absence of $GABA_A$R structural information, insights relied on analogies with related proteins. The soluble acetylcholine binding protein (AChBP) provided the first high-resolution model for the extracellular region[12]. Ground-breaking electron microscopic studies gradually led to an atomic model (at 4 Å) of a complete heteromeric nAChR from the *Torpedo marmorata* electric organ[13,14], and a general framework for molecular understanding of pLGICs. Subsequently, crystal structures of two bacterial homologues, ELIC[15] and GLIC[16], as well as the first structure of an anion-selective Cys-loop receptor, the *Caenorhabditis elegans* glutamate-gated chloride channel α homopentamer (GluClα)[17], were reported, providing insights into potential mechanisms of interaction with orthosteric ligands and allosteric modulators[17,18]. Nevertheless, owing to limited sequence identities with $GABA_A$R subunits, these models alone cannot adequately explain their rules of assembly, ligand binding and modulation, gating mechanism, or the consequences of numerous human mutations linked to epilepsy and insomnia. Aiming to address these unknowns, we report here the crystal structure of a human $GABA_A$R, the β3 homopentamer.

Architecture of the $GABA_A$R β3 homopentamer

Crystallization of human $GABA_A$R β3 required truncation of the intracellular loop between transmembrane helices 3 and 4 (M3–M4). Residues from Gly 308 to Asn 421 were substituted by a linker sequence, SQPARAA[19], to give the construct $GABA_A$R-$β3_{cryst}$ (residue numbering used here corresponds to the mature isoform 1, that is, Gln 26 in UniProt entry P28472 is Gln 1 in $GABA_A$R-$β3_{cryst}$). $GABA_A$R-$β3_{cryst}$ solubilized in detergent retained the ability to bind agonists (GABA and histamine), channel blockers (fipronil and picrotoxin) and the anaesthetic etomidate (Extended Data Fig. 1a–e). Furthermore, in patch-clamped HEK293T cells expressing $GABA_A$R-$β3_{cryst}$, application of the $GABA_A$R β3 agonists histamine or propofol induced inward currents that were inhibited by the channel blockers fipronil and picrotoxin (Extended Data Fig. 1f, g).

We crystallized and determined the structure of $GABA_A$R-$β3_{cryst}$ at 3 Å resolution (Extended Data Table 1). Viewed perpendicular to the central five-fold pseudo-symmetry axis, the receptor approximates a cylinder 110 Å in height, with diameter ranging from 60 to 80 Å (Fig. 1a), spanning the plasma membrane and protruding ~65 Å into the extracellular space. Viewed along the same pseudo-symmetry axis from the extracellular side, the pentamer has a toroidal (doughnut-like) profile, surrounded by 15 (three per subunit) N-linked glycans (Fig. 1b). Each extracellular domain (ECD) comprises an amino-terminal α-helix (α1) followed by ten β-strands folded into a curled β-sandwich, topologically similar to other family members characterized to date (Fig. 1c and Extended Data Figs 2 and 3). A second α-helix (α2), between β-strands 3 and 4, is located under the α1 helix (Fig. 1c). Four additional helices (M1–M4) from each subunit come together to create the pentameric transmembrane domain (TMD), with M2 segments lining a pore that tapers as it traverses towards the intracellular side of the membrane (Fig. 1b–d). On the extracellular side, water and solutes access the pore from a vestibule surrounded by the ECDs and from lateral tunnels situated between the ECDs that are lined by an excess of negatively charged

[1]Division of Structural Biology, Wellcome Trust Centre for Human Genetics, University of Oxford, Roosevelt Drive, Oxford OX3 7BN, UK.

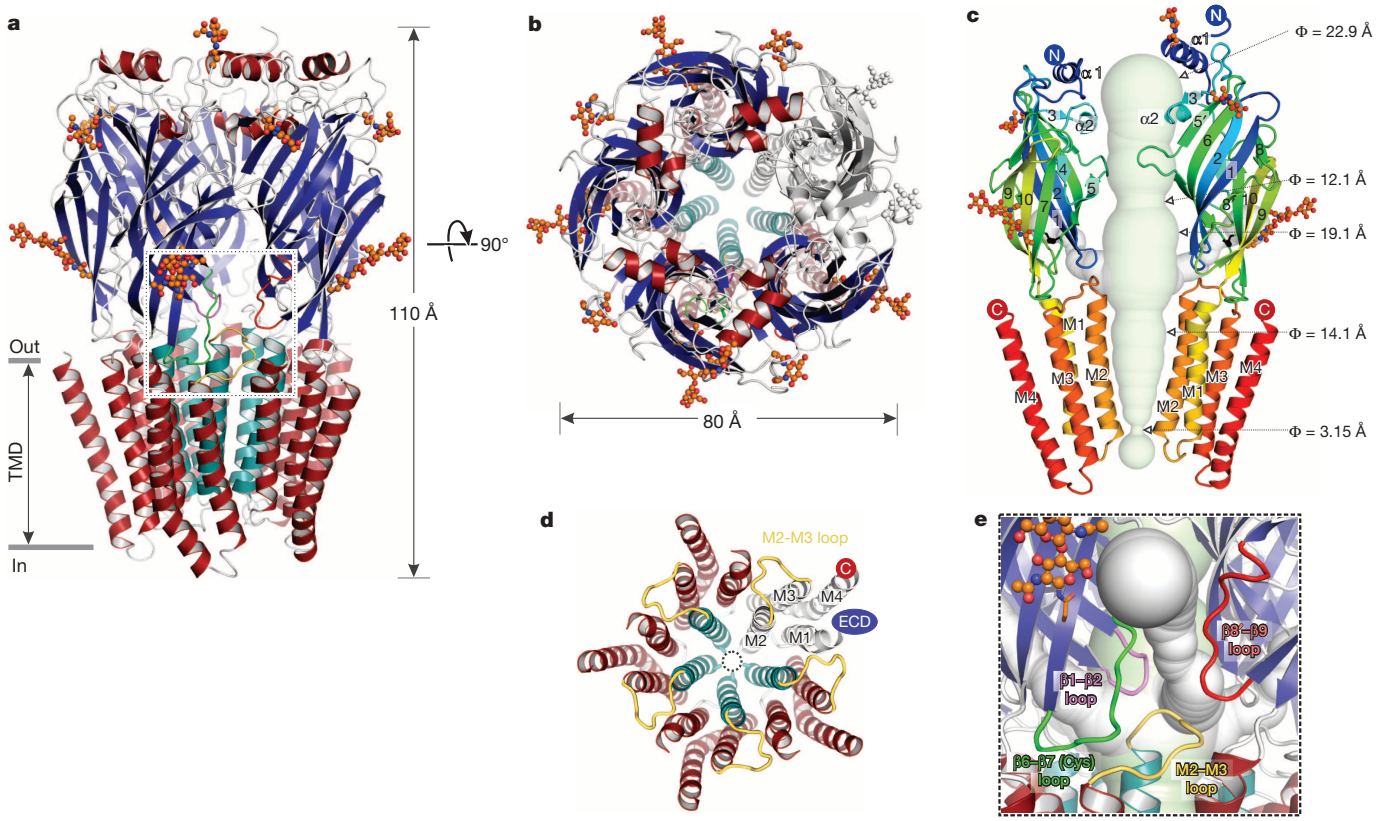

Figure 1 | Architecture of GABA$_A$R-β3$_{cryst}$. **a**, GABA$_A$R-β3$_{cryst}$ viewed parallel to the plasma membrane (α-helices red, except the pore-lining M2 shown in teal; β-strands blue; loops grey). N-linked glycans are shown in orange ball-and-stick representation. **b**, View from the extracellular space (synaptic cleft) down the five-fold pseudo-symmetry axis, with a single subunit coloured in grey. **c**, Two subunits, rainbow coloured from blue N terminus to red C terminus, illustrating secondary structure nomenclature. A water-filled ECD vestibule and TMD pore shown in light green (diameter (Φ) indicated periodically) runs through the five-fold pseudo-symmetry axis of the pentamer, joined by lateral tunnels coming from between each of the subunit ECDs (only two shown for clarity, in grey). **d**, The pentameric transmembrane region, to illustrate the arrangement of helices M1–M4 and the M2–M3 loop (yellow). **e**, View of a lateral tunnel running between subunits into the central vestibule.

groups, suggesting putative cation modulation sites (Fig. 1c, e and Extended Data Fig. 4a, d, g, h).

A positively charged ring halfway down the vestibule hosts putative anion binding sites at each inter-subunit interface (Extended Data Fig. 4d), revealed by peaks (visible to an ~6σ level) in $F_o - F_c$ electron density maps calculated following refinement without anions modelled (Extended Data Fig. 5a). Attempts to confirm the nature of these peaks by soaking heavy atom anions (for example, iodide) into the crystals and analysis of anomalous electron density maps were inconclusive. However, placement of chloride ions followed by refinement satisfactorily accounts for these electron density features (Extended Data Fig. 5a–c). This positively charged ring corresponds to the previously proposed ion selectivity filter in the vestibule of Cys-loop receptors[20]. Furthermore, these putative chloride sites are in spatial proximity (but structurally non-equivalent) to the 'anion site 1' reported in the bacterial channel GLIC[21], and thus chloride ions might be important stabilizers of pLGIC assembly.

At the TMD level, two large non-overlapping pockets are located near residues previously inferred to bind the intravenous anaesthetics etomidate and propofol[5,9] (Extended Data Fig. 6a–c). The putative propofol-binding pocket is structurally distinct from the one identified in the bacterial channel GLIC[18]. The binding and transduction modes of propofol on GABA$_A$R-β3$_{cryst}$ and GLIC are therefore unrelated, as are its relative potencies. Propofol potentiates and activates GABA$_A$Rs but inhibits GLIC[5,18].

Determinants of assembly

The 19 different GABA$_A$R subunits obey stringent rules for assembly specificity[4], the molecular determinants of which are poorly understood. A comparison of inter-subunit interfaces from pLGIC structures available to date reveals considerable differences in the geometry and thermodynamics of complex formation, with GABA$_A$R-β3$_{cryst}$ subunits forming the most extensive, energetically favourable interactions (Extended Data Fig. 7b). These occur in particular between ECDs, through patchworks of hydrogen bonds, salt bridges and van der Waals contacts (Fig. 2 a–c and Extended Data Fig. 7a–e). Within the upper portions of the ECDs, between the α1 helices of adjacent subunits, the side chains of Arg 26 and Asp 17 form a salt-bridge network extending to Asp 24 and Lys 13 (Fig. 2b), an interaction specific to β–β and α–β subunits in human GABA$_A$Rs (Extended Data Fig. 3). Between the α2 helices, the inter-subunit interface is stabilized by a network of hydrogen bonds and salt bridges surrounding Arg 86, specific to the GABA$_A$R β and GlyR subunits (Fig. 2b and Extended Data Fig. 3). The loop connecting the α1 helix with the β1 strand also bridges this interface and mutations in it (or its proximity) are associated with childhood absence epilepsy and febrile seizures[22,23] (Extended Data Fig. 3). The GABA$_A$R β3 Gly7Arg mutation that excludes γ2 subunits from heteromeric GABA$_A$Rs[22] opposes and is likely to perturb the α1–β1 loop conformation (Fig. 2b). The GABA$_A$R γ2 Arg43Gln mutation (equivalent to Arg28Gln in GABA$_A$R-β3$_{cryst}$), that also excludes γ2 subunits[23], resides within the α1–β1 loop and is predicted to disrupt its backbone organization (Fig. 2b).

Inter-subunit contacts between the central portions of ECDs involve the β4, β5, β5′ and β6 strands and flanking loops. The β5–β5′ loop is extended in GABA$_A$R-β3$_{cryst}$ and GluClα compared to nAChRs and AChBP (Extended Data Fig. 2d), and protrudes into the neighbouring subunit (Fig. 2c). The β5–β5′ loop His 107, strictly conserved in GABA$_A$ and Gly receptors, and main-chain amino groups in positions 104 and 108 coordinate putative chloride anions across this boundary (within the positively charged ring lining the vestibule discussed earlier; Fig. 2c

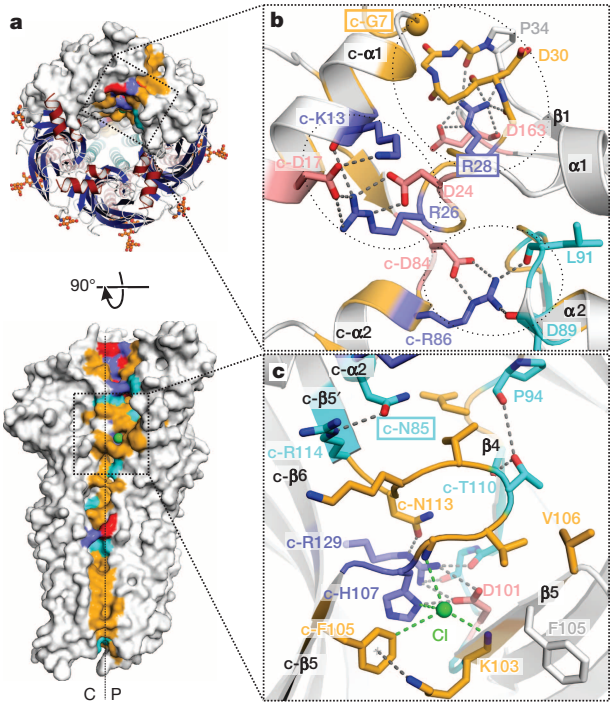

Figure 2 | Assembly interactions in $GABA_AR$-$\beta3_{cryst}$. **a**, Top-down view of the $GABA_AR$-$\beta3_{cryst}$ pentamer and side-on view of two neighbouring subunits from the vestibule, highlighting the nature of inter-subunit contacts between the principal (P) face of one subunit and complementary (C) face (residues marked by 'c-') of the next. Salt-bridging residues are coloured purple and red, those forming putative hydrogen bonds in cyan, and residues forming van der Waals contacts in orange. **b**, Upper ECD close-up showing the inter-subunit α1–β1 loop (upper dotted oval), the inter-subunit salt bridges connecting α1 helices (middle dotted oval) and inter-subunit α2–α2 interactions (lower dotted oval). Boxed residue labels correspond to disease mutations discussed in main text. **c**, The ECD anion-binding site and surrounding inter-subunit interface (chloride shown as a green sphere). Grey dashed lines indicate putative salt bridges and hydrogen bonds, green dashes indicate chloride coordination.

and Extended Data Fig. 5c). Further interface contacts include a salt-bridge network centred on Asp 101 and Arg 129, and a potential cation-π interaction between Lys 103 and Phe 105, both likely to influence assembly specificity based on residue conservation patterns (Fig. 2c and Extended Data Fig. 3). Mutations within this ECD interface are linked to epileptic encephalopathies, for example Asn85Asp[24], which will remodel interactions with basic residues adjoining the β5–β5′ loop (Fig. 2c).

Neurotransmitter pocket and binding of a novel agonist

The neurotransmitter-binding pocket of $GABA_ARs$ is located between ECDs. It comprises the β4 strand and adjacent residues (Asp 95–Leu 99), part of the β7–β8 loop (Glu 155–Tyr 159) and the β9–β10 loop (Phe 200–Tyr 205) from the 'principal' face, also known as loops A–C, respectively. The 'complementary' face in $GABA_AR$-$\beta3_{cryst}$ comprises a segment of the β2 strand (Tyr 62–Gln 64) and the β6 strand (Leu 125–Arg 129), also known as loops D and E, respectively, which come from equivalent motifs in α subunits in heteromeric $GABA_ARs$ (Fig. 3a–c and Extended Data Fig. 3)[25]. The β9–β10 loop adopts a 'closed' conformation over the site, consistent with an agonist-bound conformation[17,26–28] (Extended Data Fig. 8). Closure is stabilized by salt bridges between the side chains of Arg 207, Glu 153 and Glu 155 (Fig. 3b, c), residues previously implicated in GABA binding and channel activation[29–31]. Analogous interactions are required for ligand binding and activation of nAChRs[12,32].

We observed large positive peaks in the $F_o - F_c$ electron density map in all five neurotransmitter-binding sites, which could be accounted for by benzamidine molecules, an additive that helped us obtain high-resolution diffracting crystals (Extended Data Fig. 5d–f). To our knowledge, benzamidine or its derivatives have not been previously reported to act as $GABA_AR$ ligands. We recorded $GABA_AR$-$\beta3_{cryst}$ currents in HEK293S-GnTI$^-$ (deficient in N-acetylglucosaminyltransferase I activity) cells, and found benzamidine to behave as an agonist capable of inducing desensitization (half-maximal effective concentration (EC_{50}) = 61 ± 12 μM; n = 4; Fig. 3d, e). Thermostabilization of $GABA_AR$-$\beta3_{cryst}$ in detergent micelles by benzamidine revealed a sensitivity similar to histamine (benzamidine EC_{50} = 370 ± 180 μM; histamine EC_{50} = 400 ± 150 μM; n = 3; Fig. 3d and Extended Data Fig. 1c). Classically, benzamidine is known as a highly potent serine-protease inhibitor, derivatives of which are in clinical trials for prevention of blood clotting[33]. However, given that $GABA_AR$ β3 agonists such as histamine act instead as potentiators of heteromeric $GABA_ARs$, characterization of benzamidine derivatives as positive modulators may offer new opportunities in drug development.

The benzamidine benzyl ring is stacked between the side chains of Phe 200 and Tyr 62, whereas its amidinium group forms hydrogen bonds with the Glu 155 side chain and backbone carbonyls of Ser 156 and Tyr 157, and putative cation-π interactions with the Tyr 157 and Tyr 205 aromatic rings (Fig. 3b, c). This binding mode is reminiscent of the principal face observed in GluClα and AChBP (Extended Data Fig. 8a, b). Two epileptic encephalopathies are linked to mutations in this β3 subunit region, Asp95Asn and Glu155Gly[24]. Loss of Asp 95, which hydrogen bonds Ser 156 and Tyr 157, will probably destabilize the β7–β8 loop conformation, whereas Glu155Gly will impair binding of amino-group-containing ligands (Fig. 3b, c and Supplementary Discussion).

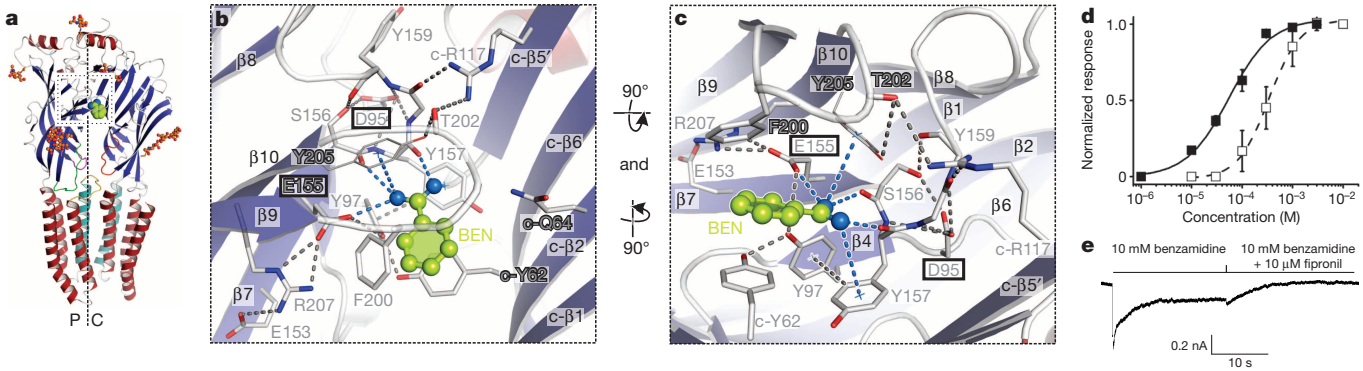

Figure 3 | Neurotransmitter pocket occupied by the agonist benzamidine. **a**, Benzamidine (green/blue spheres) bound in the neurotransmitter pocket. Of note, the β8–β8′ loop, known as loop F (Arg 169–Ala 174; running into the red loop) in heteromeric $GABA_ARs$, does not contribute to the $GABA_AR$ $\beta3_{cryst}$ orthosteric site. **b**, **c**, Benzamidine binding mode. Complementary face residues marked by 'c-'. Grey dashed lines indicate putative hydrogen bonds, salt bridges and cation-π interactions; blue dashed lines indicate the coordination sphere of benzamidine nitrogen atoms. Boxed residue labels indicate disease mutations. **d**, Benzamidine dose–response curves determined by patch-clamp of $GABA_AR$-$\beta3_{cryst}$ expressed in HEK293S-GnTI$^-$ cells (solid line) and by thermostabilization of $GABA_AR$-$\beta3_{cryst}$ in detergent micelles (dashed line; error bars are ± s.e.m.). **e**, Electrophysiological response to 10 mM benzamidine and block by 10 μM fipronil (an alternative blocker, picrotoxin, has a similar effect on $GABA_AR$-$\beta3_{cryst}$ currents; Extended Data Fig. 1d).

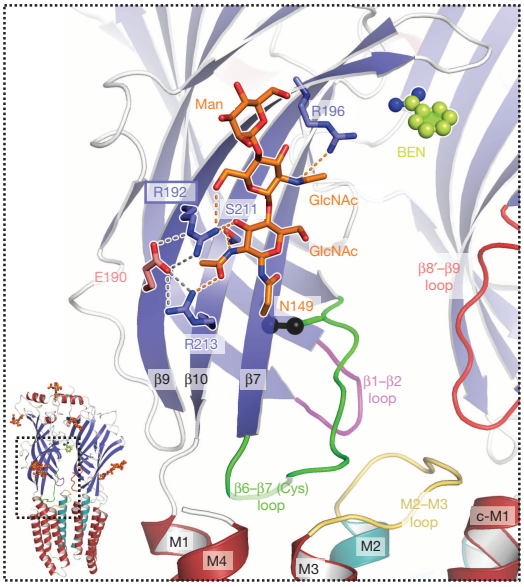

Figure 4 | A conserved glycosylation site interacts with β9–β10 loop residues. Close-up of the N-linked glycosylation site 3, attached to the β7-strand that supports the β6–β7 (Cys) loop (Cys-bridge shown in black spheres) and its interactions with surrounding residues from the β9–β10 agonist-binding loop (indicated by dashed orange lines; grey dashed lines highlight additional putative salt bridges). Boxed residue labels correspond to disease mutations discussed in main text.

The impact of N-linked glycosylation

Two of the three N-linked glycosylation sites present in each subunit (Asn 8, only visible in chain A, and Asn 80) are occupied by residual GlcNAc moieties following endoglycosidase F1 treatment. The third site, Asn 149 on the β7 strand (Fig. 4), is conserved in almost all $GABA_AR$ β, nAChR and $5HT_3R$ subunits (Extended Data Fig. 3) and was resistant to enzymatic digestion (Extended Data Fig. 5g–i). This glycan extends along the β9 and β10 strands that support the agonist-binding 'loop C', providing further contacts between these units and the β7 strand, which may facilitate the ECD–TMD signal transduction. Substitution of Asn 149 in $GABA_AR$ β2 reduces sensitivity to GABA[34], and in GlyRs, Zn^{2+} coordination between the same three β-strands potentiates agonist sensitivity[35]. Furthermore, mutation of Arg 192 at the core of this network of glycan interactions is associated with chronic insomnia and increases the inactivation rate of $GABA_ARs$[36]. Importantly, the equivalent glycan in nAChR α1 also contacts the outer face of the ECD, and its enzymatic cleavage decreases nAChR function[37].

Structural coupling between the ECD and TMD

For a neurotransmitter binding event to transmit to the channel gate, a signal must be transduced across the ECD–TMD interface. The inner and outer β-sheets of each $GABA_AR$-$β3_{cryst}$ ECD come together at the base through a conserved salt-bridge between β1–β2 loop Glu 52 and β10-strand Arg 216 (refs 14, 38) (Extended Data Fig. 7e). Beneath this, in each subunit the ECD–TMD interface consists of two clusters of interactions: an array of polar contacts linking the outer portion of the M2–M3 loop with the β6–β7 ('Cys') loop (Fig. 5a); and van der Waals contacts between residues in the inner portion of the M2–M3 loop near the pore, the β1–β2 loop and the β6–β7 loop (Fig. 5b). Central to both clusters is Pro 144 in the β6–β7 loop, conserved in all pLGICs (Extended Data Fig. 3) and adopting a *cis* conformation, which orients the neighbouring Tyr 143 backbone carbonyl downwards to engage in hydrogen bonds with M3 helix backbone amino groups (Fig. 5a). These contacts ensure that the $GABA_AR$-$β3_{cryst}$ ECD–TMD interface is tightly structurally coupled, with a solvent-inaccessible surface area of 689 $Å^2$, 100 $Å^2$ larger than observed in ELIC, but comparable to those observed in GluClα, GLIC, and the three nAChR structures solved in a membrane context by electron microscopy (Extended Data Fig. 9a). Nevertheless, despite similarly strong interfaces, structural alignments of $GABA_AR$-$β3_{cryst}$ with other pLGICs reveal differences in their ECD–TMD relative orientations, where rotations within a ~20° range probably reflect the multiplicity of states (resting, activated and desensitized) that these receptors occupy[39] (Extended Data Fig. 9b–f).

Mutations linked to epileptic encephalopathies highlight the importance of the ECD–TMD region[24,40]. One such mutation, $GABA_AR$ β3 Tyr277Cys, will reduce hydrogen-bond connectivity between the M2–M3 loop and the β6–β7 loop and disrupt a stacking interaction with the Arg 141 guanidinium group (Fig. 5a). Another mutation, $GABA_AR$ β1 Phe246Ser (Phe 221 in β3), is located at the top of M1 and will disrupt its interaction with the critical Tyr 143/Pro 144 motif at the apex of the β6–β7 loop (Fig. 5b). A Lys289Met mutation reported in $GABA_AR$ γ2 (Lys 274 in β3) affects a residue whose side chain, very well ordered in electron density maps, reaches across a neighbouring subunit (Fig. 5b and Extended Data Fig. 7e). This residue is conserved in GlyRs, for which mutations are linked to the rare human genetic startle disorder, hyperekplexia, and where detailed kinetic analysis of GlyR α1 Lys276Glu has revealed a significantly slower gating[41]. Thus, on the basis of the $GABA_AR$-$β3_{cryst}$ structure, it appears that this lysine facilitates the coordination of inter-subunit motions.

Channel structure and the desensitization mechanism

The $GABA_AR$-$β3_{cryst}$ pore is lined by five M2 helices (Fig. 1a–d), supporting 'rings' of residues between positions −5′ and 20′ (Fig. 6a). In $GABA_AR$-$β3_{cryst}$ the M2 helices taper inwards from the 13′ Thr 263

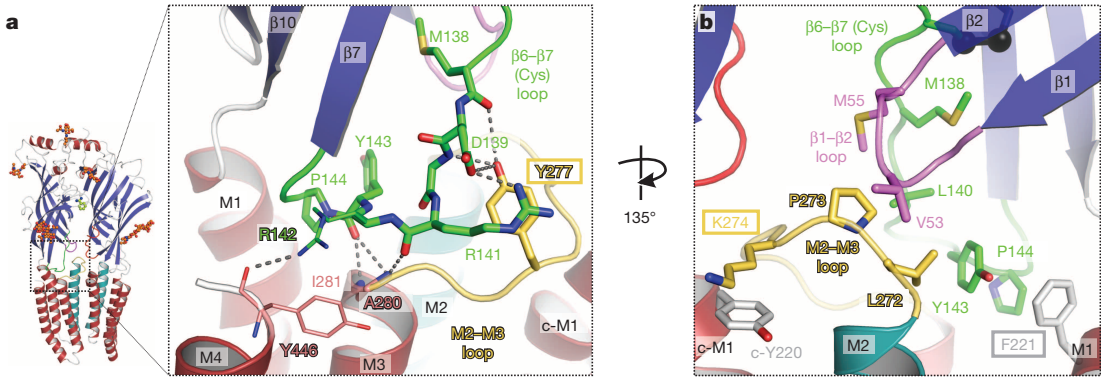

Figure 5 | Structural coupling at the ECD–TMD interface. a, Side-on view of the ECD–TMD interface, rotated 135° in **b**. **a**, Putative hydrogen bonds (indicated by grey dashed lines) between residues of the β6–β7 (Cys) loop, the outer portion of the M2–M2 loop and the top of M3 and M4 helices. **b**, Hydrophobic packing in the ECD–TMD interface viewed from the pore side, involving residues from the β6–β7 loop, the β1–β2 loop, the inner portion of the M2–M3 loop and the N terminus of the M1 helix from a neighbouring subunit (c-M1). Boxed residue labels correspond to disease mutations discussed in main text.

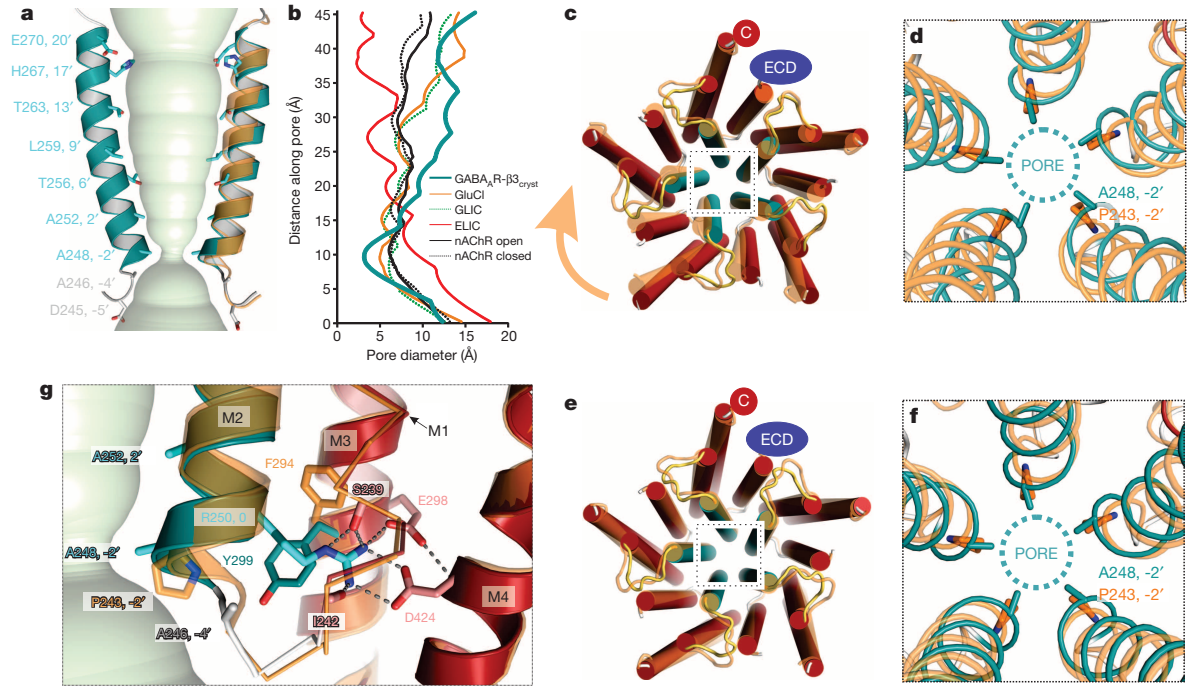

Figure 6 | Structure of the ion channel in a desensitized state. **a**, Two GABA$_A$R-β3$_{cryst}$ M2 helices (teal), with side chains of pore-lining residues in stick representation. An equivalent GluClα (Protein Data Bank (PDB) accession 3RIF) M2 helix, in orange, illustrates its distinct flexure. **b**, Pore diameter of GABA$_A$R-β3$_{cryst}$ (teal) and related structures: open GluClα, open GLIC (PDB 4HFI), open nAChR (PDB 4AQ9), closed nAChR (PDB 2BG9) and closed ELIC (PDB 2VL0). **c**, Chain A superposition of pentameric GABA$_A$R-β3$_{cryst}$ (red/teal) over GluClα (orange), revealing the relative rotation of transmembrane regions. **d**, The pore constriction at −2′ Ala 248 in GABA$_A$R-β3$_{cryst}$ compared to GluClα at −2′ Pro 243, using alignment in **c**. **e**, Superposition of individual GABA$_A$-β3$_{cryst}$ subunit TMDs over GluClα removes the relative rotation, but the pore remains shut. **f**, **g**, GABA$_A$R-β3$_{cryst}$ (red/teal) showing the Tyr 299 side-chain 'pressing' M2 to constrict the channel. In GluClα (orange) Phe 294 points upwards, enabling an open pore conformation.

down to the intracellular border where the −2′ Ala 248 side chains define the narrowest point, just 3.15 Å in diameter (Fig. 6a, b). This pore is too narrow to permit the passage of chloride anions (with a Pauling radius of 1.8 Å) and therefore delineates a closed gate. However, this geometry fundamentally differs from closed structures reported to date, ELIC[15] and *Torpedo* nAChR[14], which exhibit almost vertical M2 helices and have closed gates in the extracellular portion of the pore (9′ up to 20′) formed by bulky hydrophobic side chains (Fig. 6b). In GABA$_A$R-β3$_{cryst}$ none of the M2 hydrophobic rings (1′ Val, 3′ Leu, 5′ Ile, 8′ Val, 9′ Leu, 11′ Met, 14′ Ile and 18′ Leu) line the pore. Instead, its trajectory more closely resembles the open conformations of GLIC[16] and GluClα[17], which are narrowest at the intracellular border (Fig. 6b and Extended Data Fig. 9g).

The pore-lining residues in GABA$_A$R-β3$_{cryst}$ (Fig. 6a) are generally in excellent agreement with those identified by cysteine accessibility studies in the GABA$_A$R α1 subunit and by protonation of introduced charged residues in the open nAChR[42,43]. However, the 9′ Leu residues in GABA$_A$R-β3$_{cryst}$ (conserved across the mammalian Cys-loop receptors) are rotated out of the pore, with side chains placed between neighbouring M2 helices. This rotation is not observed in the open-to-closed M2 flexion motion in nAChR[44]. Irrespectively, the M2 rotation alone cannot explain the closed state of GABA$_A$R-β3$_{cryst}$ because superposition of each TMD individually onto the open GluClα equivalents, to remove its influence, reveals that the GABA$_A$R-β3$_{cryst}$ pore would still remain closed (Fig. 6c–f). Thus, the closed state of GABA$_A$R-β3$_{cryst}$ is principally accounted for by a unique conformation of its M2 helix (Fig. 6a and Extended Data Fig. 9g). The expanded extracellular portion of the pore in GABA$_A$R-β3$_{cryst}$ is stabilized by two rings of salt bridges. The first one involves 17′ His 267 and 20′ Glu 270 from adjacent M2 helices (Extended Data Fig. 7e). His 267 lines both the pore and an inter-subunit cavity, coordinating Zn^{2+} for inhibition or propofol for potentiation[5,45] (Extended Data Figs 6b, c and 7e). The second ring is an intra-subunit interaction between the side chains of 19′ Arg 269 and M3 Asp 282, which retracts M2 against M3 (Extended Data Fig. 7e). This ring is conserved in GABA$_A$R α-subunits and GlyR α-subunits, and substitutions of the equivalent 19′ Arg 271 in GlyR α1 are the most frequent cause of hyperekplexia, with disease mutations Arg271Leu and Arg271Gln decoupling agonist binding from gating[46].

The contracted intracellular portion of the pore is confined by the conformation of Tyr 299 side chains, which point towards the back of the M2 gate, compressing it shut (Fig. 6g). Aromatic Phe or Tyr residues occupy this position across all human GABA$_A$R and GlyR subtypes and in *C. elegans* GluClα (Extended Data Fig. 3). Notably, however, in the GluClα open pore conformation the equivalent Phe 294 side chain is rotated upwards, preventing such compression (Fig. 6g). During the gating process, conformation switching of side chains at this key position might account for local desensitization, and drugs that potentiate function by blocking desensitization[47–49] might do so by disabling this aromatic switch. A desensitized state of GABA$_A$R-β3$_{cryst}$ is in agreement with our electrophysiological recordings of benzamidine-induced desensitizing currents measured in HEK cells at saturating concentrations (10 mM), which approach those used in crystallization (33 mM; Fig. 3e). Furthermore, in heteromeric GABA$_A$Rs, swapping the β-subunit intracellular border with the equivalent nAChR α7 residues renders the receptor cation selective and ablates desensitization to GABA[50].

Conclusion

Here we present the first X-ray structure of a GABA$_A$R, the human β3 homopentamer, co-crystallized with a novel agonist, benzamidine. GABA$_A$R-β3$_{cryst}$ has a closed β9–β10 loop, being in an agonist-bound state, but the pore is shut, consistent with a desensitized conformation. To our knowledge, this is the first time when a pLGIC-desensitized state has been described crystallographically. These results shed new light on the conformational transitions that occur across pLGICs and provide a rational basis for understanding how multiple human disease mutations affect GABA$_A$R assembly, glycosylation and agonist binding, as well as the signal transduction and gating processes.

METHODS SUMMARY

$GABA_AR$-$\beta3_{cryst}$ was expressed in HEK293S-GnTI$^-$ cells and immuno-affinity purified on Rho-1D4 antibody-coated beads that bind the carboxy-terminal 1D4 tag (TETSQVAPA). Pure $GABA_AR$-$\beta3_{cryst}$ was further isolated by size-exclusion chromatography and peak fractions were concentrated to 3 mg ml^{-1}. Crystallization was performed by sitting-drop vapour diffusion at 4 °C with a precipitating solution containing 11.5% PEG 4000, 100 mM NaCl, 100 mM Li_2SO_4, 100 mM N-(2-Acetamido)iminodiacetic acid buffer, pH 6.5, and 2% (v/w) benzamidine. Crystals were cryoprotected by soaking in precipitant solution supplemented with 20% glycerol. The $GABA_AR$-$\beta3_{cryst}$ X-ray structure was solved at 3 Å resolution, using the *C. elegans* glutamate-gated chloride channel α (GluClα[17]) as a molecular replacement model. Phasing was followed by iterative rounds of manual model building and crystallographic refinement, leading to a complete model of the protein core. N-linked glycans, anions and benzamidine were subsequently added to the model and refined. Electrophysiological recordings were made from either transiently transfected HEK293T cells or HEK293S-GnTI$^-$ cells stably expressing $GABA_AR$-$\beta3_{cryst}$.

Online Content Any additional Methods, Extended Data display items and Source Data are available in the online version of the paper; references unique to these sections appear only in the online paper.

Received 15 December 2013; accepted 28 March 2014.
Published online 8 June 2014.

1. Rabow, L. E., Russek, S. J. & Farb, D. H. From ion currents to genomic analysis: recent advances in GABAA receptor research. *Synapse* **21,** 189–274 (1995).
2. Grenningloh, G. *et al.* Glycine vs GABA receptors. *Nature* **330,** 25–26 (1987).
3. Simon, J., Wakimoto, H., Fujita, N., Lalande, M. & Barnard, E. A. Analysis of the set of $GABA_A$ receptor genes in the human genome. *J. Biol. Chem.* **279,** 41422–41435 (2004).
4. Sigel, E. & Steinmann, M. E. Structure, function, and modulation of $GABA_A$ receptors. *J. Biol. Chem.* **287,** 40224–40231 (2012).
5. Yip, G. M. *et al.* A propofol binding site on mammalian $GABA_A$ receptors identified by photolabeling. *Nature Chem. Biol.* **9,** 715–720 (2013).
6. Karlin, A. & Akabas, M. H. Toward a structural basis for the function of nicotinic acetylcholine receptors and their cousins. *Neuron* **15,** 1231–1244 (1995).
7. Miller, P. S. & Smart, T. G. Binding, activation and modulation of Cys-loop receptors. *Trends Pharmacol. Sci.* **31,** 161–174 (2010).
8. Rudolph, U. & Knoflach, F. Beyond classical benzodiazepines: novel therapeutic potential of $GABA_A$ receptor subtypes. *Nature Rev. Drug Discov.* **10,** 685–697 (2011).
9. Li, G. D. *et al.* Identification of a $GABA_A$ receptor anesthetic binding site at subunit interfaces by photolabeling with an etomidate analog. *J. Neurosci.* **26,** 11599–11605 (2006).
10. Wallner, M., Hanchar, H. J. & Olsen, R. W. Ethanol enhances $\alpha_4\beta_3\delta$ and $\alpha_6\beta_3\delta$ γ-aminobutyric acid type A receptors at low concentrations known to affect humans. *Proc. Natl Acad. Sci. USA* **100,** 15218–15223 (2003).
11. Belelli, D. & Lambert, J. J. Neurosteroids: endogenous regulators of the $GABA_A$ receptor. *Nature Rev. Neurosci.* **6,** 565–575 (2005).
12. Brejc, K. *et al.* Crystal structure of an ACh-binding protein reveals the ligand-binding domain of nicotinic receptors. *Nature* **411,** 269–276 (2001).
13. Miyazawa, A., Fujiyoshi, Y. & Unwin, N. Structure and gating mechanism of the acetylcholine receptor pore. *Nature* **423,** 949–955 (2003).
14. Unwin, N. Refined structure of the nicotinic acetylcholine receptor at 4 Å resolution. *J. Mol. Biol.* **346,** 967–989 (2005).
15. Hilf, R. J. & Dutzler, R. X-ray structure of a prokaryotic pentameric ligand-gated ion channel. *Nature* **452,** 375–379 (2008).
16. Bocquet, N. *et al.* X-ray structure of a pentameric ligand-gated ion channel in an apparently open conformation. *Nature* **457,** 111–114 (2009).
17. Hibbs, R. E. & Gouaux, E. Principles of activation and permeation in an anion-selective Cys-loop receptor. *Nature* **474,** 54–60 (2011).
18. Nury, H. *et al.* X-ray structures of general anaesthetics bound to a pentameric ligand-gated ion channel. *Nature* **469,** 428–431 (2011).
19. Jansen, M., Bali, M. & Akabas, M. H. Modular design of Cys-loop ligand-gated ion channels: functional 5–HT_3 and GABA ρ1 receptors lacking the large cytoplasmic M3M4 loop. *J. Gen. Physiol.* **131,** 137–146 (2008).
20. Hansen, S. B., Wang, H. L., Taylor, P. & Sine, S. M. An ion selectivity filter in the extracellular domain of Cys-loop receptors reveals determinants for ion conductance. *J. Biol. Chem.* **283,** 36066–36070 (2008).
21. Sauguet, L. *et al.* Structural basis for ion permeation mechanism in pentameric ligand-gated ion channels. *EMBO J.* **32,** 728–741 (2013).
22. Gurba, K. N., Hernandez, C. C., Hu, N. & Macdonald, R. L. *GABRB3* mutation, G32R, associated with childhood absence epilepsy alters $\alpha_1\beta_3\gamma_2$L γ-aminobutyric acid type A ($GABA_A$) receptor expression and channel gating. *J. Biol. Chem.* **287,** 12083–12097 (2012).
23. Sancar, F. & Czajkowski, C. A $GABA_A$ receptor mutation linked to human epilepsy (γ_2R43Q) impairs cell surface expression of αβγ receptors. *J. Biol. Chem.* **279,** 47034–47039 (2004).
24. Epi, K. C. *et al. De novo* mutations in epileptic encephalopathies. *Nature* **501,** 217–221 (2013).
25. Bergmann, R., Kongsbak, K., Sorensen, P. L., Sander, T. & Balle, T. A Unified model of the $GABA_A$ receptor comprising agonist and benzodiazepine binding sites. *PLoS ONE* **8,** e52323 (2013).
26. Hansen, S. B. *et al.* Structures of *Aplysia* AChBP complexes with nicotinic agonists and antagonists reveal distinctive binding interfaces and conformations. *EMBO J.* **24,** 3635–3646 (2005).
27. Huang, S. *et al.* Complex between α-bungarotoxin and an α7 nicotinic receptor ligand-binding domain chimaera. *Biochem. J.* **454,** 303–310 (2013).
28. Celie, P. H. *et al.* Nicotine and carbamylcholine binding to nicotinic acetylcholine receptors as studied in AChBP crystal structures. *Neuron* **41,** 907–914 (2004).
29. Newell, J. G., McDevitt, R. A. & Czajkowski, C. Mutation of glutamate 155 of the $GABA_A$ receptor β_2 subunit produces a spontaneously open channel: a trigger for channel activation. *J. Neurosci.* **24,** 11226–11235 (2004).
30. Venkatachalan, S. P. & Czajkowski, C. A conserved salt bridge critical for $GABA_A$ receptor function and loop C dynamics. *Proc. Natl Acad. Sci. USA* **105,** 13604–13609 (2008).
31. Wagner, D. A., Czajkowski, C. & Jones, M. V. An arginine involved in GABA binding and unbinding but not gating of the $GABA_A$ receptor. *J. Neurosci.* **24,** 2733–2741 (2004).
32. Mukhtasimova, N., Free, C. & Sine, S. M. Initial coupling of binding to gating mediated by conserved residues in the muscle nicotinic receptor. *J. Gen. Physiol.* **126,** 23–39 (2005).
33. Rees, D. C., Congreve, M., Murray, C. W. & Carr, R. Fragment-based lead discovery. *Nature Rev. Drug Discov.* **3,** 660–672 (2004).
34. Lo, W. Y. *et al.* Glycosylation of β2 subunits regulates $GABA_A$ receptor biogenesis and channel gating. *J. Biol. Chem.* **285,** 31348–31361 (2010).
35. Miller, P. S., Da Silva, H. M. & Smart, T. G. Molecular basis for zinc potentiation at strychnine-sensitive glycine receptors. *J. Biol. Chem.* **280,** 37877–37884 (2005).
36. Buhr, A. *et al.* Functional characterization of the new human $GABA_A$ receptor mutation β3(R192H). *Hum. Genet.* **111,** 154–160 (2002).
37. Dellisanti, C. D., Yao, Y., Stroud, J. C., Wang, Z. Z. & Chen, L. Crystal structure of the extracellular domain of nAChR α1 bound to α-bungarotoxin at 1.94 Å resolution. *Nature Neurosci.* **10,** 953–962 (2007).
38. Lee, W. Y. & Sine, S. M. Principal pathway coupling agonist binding to channel gating in nicotinic receptors. *Nature* **438,** 243–247 (2005).
39. Akabas, M. H. Using molecular dynamics to elucidate the structural basis for function in pLGICs. *Proc. Natl Acad. Sci. USA* **110,** 16700–16701 (2013).
40. Baulac, S. *et al.* First genetic evidence of $GABA_A$ receptor dysfunction in epilepsy: a mutation in the γ2-subunit gene. *Nature Genet.* **28,** 46–48 (2001).
41. Lape, R., Plested, A. J., Moroni, M., Colquhoun, D. & Sivilotti, L. G. The α1K276E startle disease mutation reveals multiple intermediate states in the gating of glycine receptors. *J. Neurosci.* **32,** 1336–1352 (2012).
42. Xu, M. & Akabas, M. H. Identification of channel-lining residues in the M2 membrane-spanning segment of the $GABA_A$ receptor alpha1 subunit. *J. Gen. Physiol.* **107,** 195–205 (1996).
43. Cymes, G. D., Ni, Y. & Grosman, C. Probing ion-channel pores one proton at a time. *Nature* **438,** 975–980 (2005).
44. Unwin, N. & Fujiyoshi, Y. Gating movement of acetylcholine receptor caught by plunge-freezing. *J. Mol. Biol.* **422,** 617–634 (2012).
45. Horenstein, J. & Akabas, M. H. Location of a high affinity Zn^{2+} binding site in the channel of α1β1 γ-aminobutyric $acid_A$ receptors. *Mol. Pharmacol.* **53,** 870–877 (1998).
46. Rajendra, S. *et al.* Mutation of an arginine residue in the human glycine receptor transforms β-alanine and taurine from agonists into competitive antagonists. *Neuron* **14,** 169–175 (1995).
47. Young, G. T., Zwart, R., Walker, A. S., Sher, E. & Millar, N. S. Potentiation of α7 nicotinic acetylcholine receptors via an allosteric transmembrane site. *Proc. Natl Acad. Sci. USA* **105,** 14686–14691 (2008).
48. daCosta, C. J., Free, C. R., Corradi, J., Bouzat, C. & Sine, S. M. Single-channel and structural foundations of neuronal α7 acetylcholine receptor potentiation. *J. Neurosci.* **31,** 13870–13879 (2011).
49. Shan, Q., Haddrill, J. L. & Lynch, J. W. Ivermectin, an unconventional agonist of the glycine receptor chloride channel. *J. Biol. Chem.* **276,** 12556–12564 (2001).
50. Jensen, M. L. *et al.* The β subunit determines the ion selectivity of the $GABA_A$ receptor. *J. Biol. Chem.* **277,** 41438–41447 (2002).

Supplementary Information is available in the online version of the paper.

Acknowledgements We thank T. Malinauskas, Y. Kong and staff at Diamond Light Source beamlines I03 and I24 for synchrotron assistance; K. Harlos and T. Walter for technical support with crystallization; G. Schertler and J. Standfuss for advice concerning the Rho-1D4 affinity purification method; T. Nakagawa for electron microscopy sample examination; F. Ashcroft, S. Tucker, M. Clausen and P. Proks for access to electrophysiology equipment and assistance with electrophysiological recordings; J. McIlhinney, M. Sansom, L. Carpenter, S. Newstead, I. de Moraes and members of the Aricescu laboratory for discussions; E.Y. Jones, D.I. Stuart and C. Siebold for reading the manuscript. This work was supported by grants from the Wellcome Trust (OXION: Ion channels and Disease Initiative, 084655), the UK Medical Research Council ((MRC) G0700232) and the Royal Society (RG090810). Further support from the Wellcome Trust Core Award Grant Number 090532/Z/09/Z is acknowledged. P.S.M. was a Wellcome Trust OXION Training Fellow. A.R.A. is an MRC Senior Research Fellow.

Author Contributions The authors have jointly contributed to the project design, data analysis and manuscript preparation. Experimental work was performed by P.S.M. (protein expression, purification, crystallization, ligand binding assays and electrophysiology) and A.R.A. (crystallography).

Author Information The coordinates and the structure factors have been deposited in the Protein Data Bank under the accession code 4COF. Reprints and permissions information is available at www.nature.com/reprints. The authors declare competing financial interests: details can be found in the online version of the paper. Readers are welcome to comment on the online version of the paper. Correspondence and requests for materials should be addressed to A.R.A. (radu@strubi.ox.ac.uk) or P.S.M. (paul@strubi.ox.ac.uk).